Mathematical modeling of intracellular and intratissue activities for understanding dynamic optical coherence tomography signals

Yuanke Feng[1], Shumpei Fujimura[1], Yiheng Lim[1], Thitiya Seesan[1], Rion Morishita[1], Ibrahim Abd El-Sadek[1,2], Pradipta Mukherjee[1] and Yoshiaki Yasuno[1]

[1]*Computational Optics Group, University of Tsukuba, Japan,* [2]*Faculty of Science, Damietta University, Egypt*

ABSTRACT

Dynamic optical coherence tomography (DOCT) is developed to evaluate the functional activities of wide spectrum of tissues. However, the relation between the DOCT signals and the intracellular motion is not fully identified yet. This unidentified relationship inhibits further dissemination of DOCT signals.

In this study, we proposed a theoretical and numerical framework to understand DOCT. It includes the classification of intracellular motility, their mathematical modeling, and numerical simulation. We classified intracellular motilities into six types: active transport, passive transport, jiggling, floating of dissociated cells, migration, and flow. Then, the motilities were modeled by three physical models: flow, random ballistic and diffusion. The sample motion and it resulting time-sequential OCT images were numerically simulated. Two DOCT contrasts were computed from the OCT time-sequence: logarithmic intensity variance of OCT (LIV) and temporal variance of complex OCT signals (complex variance).

We considered the random ballistic motions measured by two different probing wavelengths of 840 nm and 1310 nm. Tessellated pattern of low and high LIV was found in LIV images. The LIV and complex variance increase within the velocity range of 4.5 to 270 nm/s, while it becomes almost constant for larger velocities. Additionally, we found that both LIV and complex variance are higher when shorter wavelength is considered.

Using the proposed theoretical model, we can better understand the specific intracellular tissue activities that contribute to the high DOCT signal.

Keywords: Dynamic optical coherence tomography, dynamic scattering, mathematical modeling, intracellular activities, wave optics simulation, speckle.

INTRODUCTION

Optical coherence tomography (OCT) is a three dimensional (3D) imaging modality that provide non-invasive and high-resolution imaging of the microstructure of biological tissues[1]. Recently, dynamic optical coherence tomography (DOCT) is developed for label-free assessment of tissue functional activity[2]. It has been used for the evaluation of tissue activity for wide spectrum of tissues, including *in vitro* tumor spheroid[2], organoid[3], and fresh *ex vivo* animal tissues[4].

DOCT quantifies the temporal fluctuation of OCT signals, which is believed to be originated from the intracellular motility. However, there are numerous types of intracellular motility and the relation between the DOCT signals and the type of intracellular motion is not fully identified yet. This unidentified relationship inhibits further development of DOCT imaging.

In this study, we proposed a DOCT signal simulator using mathematical modeling of intracellular activities. First, we classified the intracellular tissue activities into six categories. Second, we mathematically modeled the intracellular activities by using several physical models. Third, we performed numerical simulation by using the mathematical model to recapitulate the specific temporal fluctuation of OCT signals caused by the cellular and tissue activities. Then, with this simulated OCT, two DOCT contrasts were computed: the logarithmic intensity variance (LIV) and complex variance. And the relationship between the DOCT signals and the tissue activities was investigated.

MODELING OF INTRACELLULAR DYNAMICS

2.1. Classification of intracellular dynamics

We classified the intracellular activities into six categories, including active transport, passive transport, intracellular jiggling, dissociation of floaters, cell migration and flow of intracellular fluids. For each category, we proposed a corresponding physical dynamic model to describe the motion of the scatterers as follows.

First, active transport is defined as the movement of molecules across a cell membrane from a region of lower concentration to a region of higher concentration[5]. And dissociation of floaters is considered as the diffusion of the

intracellular organelles to the extracellular space during apoptosis[6]. We consider the above two categories follow a random ballistic model.

Second, passive transport, which is defined as the membrane transport that does not require energy to move substance[7], and intracellular jiggling can be considered as the diffusion model. The intracellular constituents of the jiggling are organelles[8].

Third, cell migration is a vital process in the development and maintenance of multicellular organisms[9]. We describe it as a combination of mono-direction translation and diffusion. And fluid flow is directed from the cell body towards the cell edge[10]. We describe the intracellular fluid flow as a mono-direction translation.

2.2. Physical models for the tissue dynamics

To simulate time dynamics of scatterers, we considered three typical models, including mono-direction translation, random ballistic model, and diffusion. The mathematical details of the models are following.

2.2.1 Mono-direction translation

For mono-direction ballistic motion model, we assume all the scatterers follow uniform linear motion and both the velocity amplitude and the velocity angle are same for all the scatterers. Therefore, the temporal location change of scatterers is expressed as

$$\begin{aligned} x_{j,i+1} - x_{j,i} &= v \sin\varphi \cos\theta \, (t_{i+1} - t_i), \\ y_{j,i+1} - y_{j,i} &= v \sin\varphi \sin\theta \, (t_{i+1} - t_i), \\ z_{j,i+1} - z_{j,i} &= v \cos\varphi \, (t_{i+1} - t_i), \end{aligned} \tag{1}$$

where $x_{j,i}, y_{j,i}, z_{j,i}$ represents the location of j-th scatterer at time point t_i, v represents the amplitude of the velocity, φ and θ represent the azimuth and inclination angles of the scatterer motion.

2.2.2 Diffusion

For diffusion motion model, the displacement increments of the scatterers in each dimension obey the zero-mean normal distribution, whereas the variance of the displacement of the scatterers can be expressed as

$$\langle (x_{j,i+1} - x_{j,i})^2 \rangle_j = 2D(t_{i+1} - t_i), \tag{2}$$

where $x_{j,i}$ represents the location of j-th particle at time point t_i, $\langle \quad \rangle_j$ is the average over all the scatterers. For y and z directions, the variance follows the same equation.

2.2.3 Random ballistic motion

For random ballistic motion model, we assume all the scatterers follow uniform linear motion and the velocity amplitude is same for all the scatterers, but the directions of motion are randomized. Therefore, the temporal location change of scatterers is expressed as

$$\begin{aligned} x_{j,i+1} - x_{j,i} &= v \sin\varphi_j \cos\theta_j \, (t_{i+1} - t_i), \\ y_{j,i+1} - y_{j,i} &= v \sin\varphi_j \sin\theta_j \, (t_{i+1} - t_i), \\ z_{j,i+1} - z_{j,i} &= v \cos\varphi_j \, (t_{i+1} - t_i), \end{aligned} \tag{3}$$

where $x_{j,i}, y_{j,i}, z_{j,i}$ represents the location of j-th scatterer at time point t_i, v represents the amplitude of the velocity, φ_j, θ_j represent the azimuth and inclination of the motion of j-th scatterer.

NUMERICAL SIMULATION

3.1. Scatterer simulation scheme

We assume scatterers are moving by following the proposed physical dynamics model. After inter-frame interval Δt, the scatterers move from the location $(x_{j,i}, y_{j,i}, z_{j,i})$ at time-point t_i to the location $(x_{j,i+1}, y_{j,i+1}, z_{j,i+1})$ at next time-point t_{i+1}. Assuming the light incident from z = 0, which is the upper surface of the simulation field, and initial phase of the light is 0 on the upper surface, the phase of the electric field contribution to the OCT signal from each scatterer can be derived from the axial location $z_{j,i}$. We divide the entire volume by a voxel of a particular size. Therefore, multiple particles likely to be located in the same voxel. And the electric field of the m-th voxel which locates at (x_m, y_m, z_m) is defined as

$$E(x_m, y_m, z_m) = \sum_{j,i \in \mathrm{m-th\ voxel}} r_{j,i} \cdot \exp\left[i \frac{4\pi n z_{j,i}}{\lambda} \right], \tag{4}$$

where $\sum_{j,i\in \mathrm{m-th\ voxel}}$ means summation over all scatterers located in the m-th voxel at time point t_i, $r_{j,i}$ is the amplitude reflectivity of the j-th particles at time point t_i, λ is the wavelength of the incident light, n is the relative refractive index of the medium, and $2nz_{j,i}$ represents the round-trip optical path length of reflected light. Meanwhile, the intensity distribution is computed as $S(x,y,z) = E(x,y,z)E(x,y,z)^*$.

Then, we numerically generate a 3-D point spread function PSF(x,y,z) which is assumed to be 3-D Gaussian[11]. The axial and lateral resolution are selected manually based on two custom-built OCT system. Then the speckle pattern can be computed by convolving the intensity distribution with the PSF as

$$\mathrm{I}(x,y,z) = \mathrm{S}(x,y,z) * \mathrm{PSF}(x,y,z)\,, \tag{5}$$

where * indicates 3D convolution.

3.2. Implementation

3.2.1 Simulation protocol

Our simulation simulated the particle motion and OCT signal within the time duration T, which was 6348.8 ms. We assumed that 32 OCT frames are repeatedly acquired and the inter-frame interval $\Delta t = (\mathrm{t_{i+1}} - \mathrm{t_i})$ is 204.8 ms. We considered two OCT systems whose specifications are summarized in Table 1.

Table 1: System parameter used in simulations.

Parameter	System1	System2
Center probe wavelength [nm]	1310	840
Axial resolution [μm]	14	4.9
Lateral resolution [μm]	18	3.8
Grid size [μm/pixel]	1.95 × 1.95 × 7.24	1.95 × 1.95 × 2.5
Pixel number	100 × 100 × 100	100 × 100 × 100
Analytic field size [μm^3]	195 × 195 × 724	195 × 195 × 250
Total scatter field size [μm^3]	345 × 345 × 874	345 × 345 × 400
Scatterer density [μm^{-3}]	1	1

3.2.2 DOCT algorithm

We computed two DOCT contrasts from the simulated time-sequence of OCT signals. One is the logarithmic intensity variance (LIV). LIV is defined as time variance of the time sequential logarithmic (dB-scaled) OCT intensity signals[12]. The other is complex variance, which is defined as the summation of temporal variances of the real and imaginary components of the complex OCT signal. Finally, we compared the results with different simulation parameters.

3.3. Result

Figure 1(a) shows representative frames of an OCT B-scan sequence simulated with the random ballistic model with the parameters of system 1. The time interval of adjacent frames is 204.8 ms and the scatterers' velocity amplitude is 225 nm/s. Figure 1(b) shows pseudo-colored B-scan LIV image. According to Fig. 1, we found the local speckle pattern highly morphs by the random ballistic motion. The LIV image exhibits heterogeneous structure of high and low LIV.

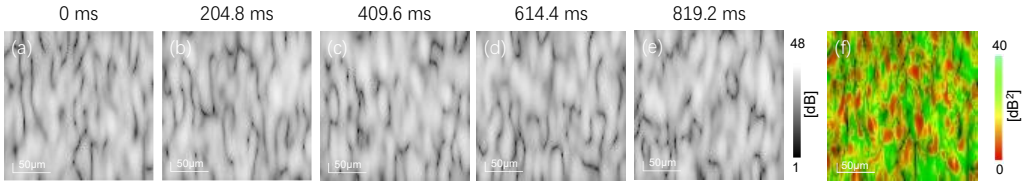

Figure 1: (a-e) Representative frames of a sequential cross-sectional OCT. The speckle pattern is decorrelated by the diffusive motion of the scatterers. (f) The cross-sectional LIV computed from the OCT sequence.

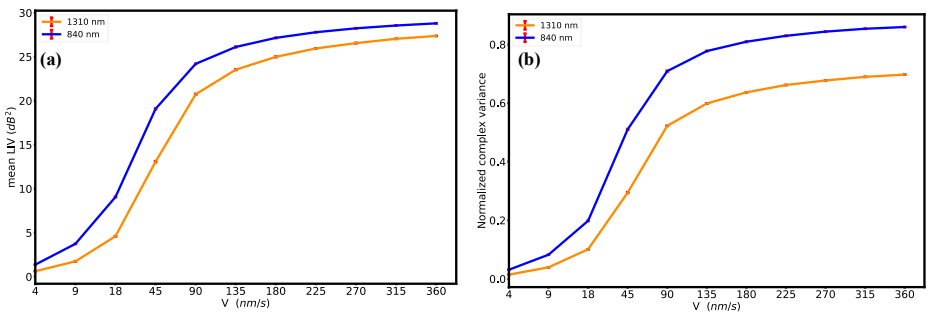

Figure 2: Simulation suggests that the both LIV (a) and normalized complex variance (b) monotonically increase as the scatters' velocity increases in the random ballistic model. In addition, both of them have non-negligible system (wavelength and resolution) dependency.

Figure 2(a) and 2(b) respectively show a mean LIV and normalized complex signal variance versus different amplitude of velocity, where the scatterers are assumed to follow the random ballistic model. The complex variance is normalized by the temporal average of the OCT intensity. Each point is the mean of 8 trials and the error bar shows the standard deviation. It was found that the two DOCT signals first increase as the velocity increases and then reaches a plateau for both the two systems. It indicates that the LIV and normalized complex variance are sensitive to the magnitude of scatterer velocity. Additionally, the system 2, which has shorter probe wavelength and higher resolution than system 1, gave higher mean LIV and normalized complex variance. It suggests LIV and the normalized complex variance may depend on the wavelength and resolution.

CONCLUSION

In this study we classified the intracellular activities into six categories and modeled them by physical models and their combinations. We simulated scatterers' motion and computed time-sequential OCT signal, and two DOCT contrasts were computed. The simulation revealed that the LIV and the normalized complex variance are sensitive to the magnitude of scatterer velocity. In addition, they are affected by the probe wavelength and the resolution. Using the proposed theoretical model, we can better understand the specific intracellular tissue activities that contribute to the high DOCT signal.

REFERENCES

[1] Schmitt, J. M., "Optical coherence tomography (OCT): a review," IEEE J. Sel. Top. Quantum Electron. **5**(4), 1205–1215 (1999).

[2] El-Sadek, I. A., Miyazawa, A., Shen, L. T.-W., Makita, S., Mukherjee, P., Lichtenegger, A., Matsusaka, S. and Yasuno, Y., "Three-dimensional dynamics optical coherence tomography for tumor spheroid evaluation," Biomed. Opt. Express **12**(11), 6844–6863 (2021).

[3] Morishita, R., Suzuki, T., Mukherjee, P., El-Sadek, I. A., Lim, Y., Lichtenegger, A., Makita, S., Tomita, K., Yamamoto, Y., Nagamoto, T. and Yasuno, Y., "Label-free intratissue activity imaging of alveolar organoids with dynamic optical coherence tomography," Biomed. Opt. Express **14**(5), 2333–2351 (2023).

[4] Mukherjee, P., Miyazawa, A., Fukuda, S., Yamashita, T., Lukmanto, D., Okada, K., El-Sadek, I. A., Zhu, L., Makita, S., Oshika, T. and Yasuno, Y., "Label-free functional and structural imaging of liver microvascular complex in mice by Jones matrix optical coherence tomography," 1, Sci. Rep. **11**(1), 20054 (2021).

[5] Bressloff, P. C. and Newby, J. M., "Stochastic models of intracellular transport," Rev. Mod. Phys. **85**(1), 135–196 (2013).

[6] Bagchi, A. K., Malik, A., Akolkar, G., Zimmer, A., Belló-Klein, A., De Angelis, K., Jassal, D. S., Fini, M. A., Stenmark, K. R. and Singal, P. K., "Study of ER stress and apoptotic proteins in the heart and tumor exposed to doxorubicin," Biochim. Biophys. Acta BBA - Mol. Cell Res. **1868**(7), 119039 (2021).

[7] Arcizet, D., Meier, B., Sackmann, E., Rädler, J. O. and Heinrich, D., "Temporal Analysis of Active and Passive Transport in Living Cells," Phys. Rev. Lett. **101**(24), 248103 (2008).

[8] van der Honing, H. S., de Ruijter, N. C. A., Emons, A. M. C. and Ketelaar, T., "Actin and myosin regulate cytoplasm stiffness in plant cells: a study using optical tweezers," New Phytol. **185**(1), 90–102 (2010).

[9] Wortel, I. M. N., Liu, A. Y., Dannenberg, K., Berry, J. C., Miller, M. J. and Textor, J., "CelltrackR: An R package for fast and flexible analysis of immune cell migration data," ImmunoInformatics **1–2**, 100003 (2021).

[10] Keren, K., Yam, P. T., Kinkhabwala, A., Mogilner, A. and Theriot, J. A., "Intracellular fluid flow in rapidly moving cells," 10, Nat. Cell Biol. **11**(10), 1219–1224 (2009).

[11] Seesan, T., El-Sadek, I. A., Mukherjee, P., Zhu, L., Oikawa, K., Miyazawa, A., Shen, L. T.-W., Matsusaka, S., Buranasiri, P., Makita, S. and Yasuno, Y., "Deep convolutional neural network-based scatterer density and resolution estimators in optical coherence tomography," Biomed. Opt. Express **13**(1), 168–183 (2022).

[12] El-Sadek, I. A., Miyazawa, A., Shen, L. T.-W., Makita, S., Fukuda, S., Yamashita, T., Oka, Y., Mukherjee, P., Matsusaka, S., Oshika, T., Kano, H. and Yasuno, Y., "Optical coherence tomography-based tissue dynamics imaging for longitudinal and drug response evaluation of tumor spheroids," Biomed. Opt. Express **11**(11), 6231–6248 (2020).